Circulation Research

ORIGINAL RESEARCH

Circulating Immune Cell Signature Analysis in HFpEF Across Species

Jasmin M. Kneuer, Marion Müller, Stephan Erbe, Karoline E. Kokot, Sebastian Rosch, Irina Müller-Kozarez, Sophie Charlotte Schrö, Christina Maeder, Sarah Felicitas Heitkamp, Susanne Gaul, Stephan von Haehling, Anke Tönjes, Matthias Blüher, Philipp Lurz, Rolf Wachter, Anna Klinke, Ulrich Laufs, Jes-Niels Boeckel

BACKGROUND: Heart failure with preserved ejection fraction (HFpEF) is a heterogeneous clinical picture that is closely related to extracardiac comorbidities such as obesity, hypertension, and diabetes and is associated with chronic, low-grade systemic inflammation. Previous studies on myocardial biopsies of patients with HFpEF showed intramyocardial inflammatory activity, suggesting that the inflammatory processes in HFpEF are predominantly systemic and exhibit compartment-specific patterns.

METHODS: We performed single-cell RNA sequencing of peripheral blood mononuclear cells of patients with HFpEF (n=6), heart failure with reduced ejection fraction patients (n=8), and healthy controls (n=7), taking obesity status into account. For validation, bulk RNA sequencing was performed on whole blood samples. In parallel, the systemic immune cell response was investigated in an HFpEF mouse model (induced by a high-fat diet plus L-NAME), with one group additionally administered the anti-inflammatory agent nitro-oleic acid.

RESULTS: Analysis of human peripheral blood mononuclear cells revealed an HFpEF-specific inflammatory fingerprint, which manifested in obesity-related increased expression of cytokine signaling genes (eg, *CCL2* and *TNF*) and obesity-independent increases in mitochondrial-associated activity. In the mouse model, HFpEF animals showed a comparable increase in inflammatory markers, with treatment with nitro-oleic acid leading to a partial normalization of immunologic signatures and a significant improvement in diastolic function.

CONCLUSIONS: Our results demonstrate that the immune cells of patients with HFpEF are characterized by a distinct transcriptional immune signature that differs from that of patients with heart failure with reduced ejection fraction analyzed in this study. The conserved immunologic signatures between the human and murine data sets analyzed here, and the beneficial effect of nitro-oleic acid in the preclinical model induced by high-fat diet and L-NAME, provide translational insights and generate hypotheses for personalized interventions in HFpEF.

GRAPHIC ABSTRACT: A graphic abstract is available for this article.

Key Words: heart failure ■ hypertension ■ inflammation ■ microcirculation ■ stroke volume

Heart failure with preserved ejection fraction (HFpEF) accounts for about half of all cases of heart failure and is characterized by diastolic dysfunction, increased myocardial stiffness, and an unfavorable prognosis. In contrast to heart failure with reduced ejection fraction (HFrEF), which is caused by an inside-out mechanism following direct myocardial damage (eg, myocardial infarction), HFpEF is mainly caused by extracardiac comorbidities such as obesity, hypertension, and diabetes.[1,2] These diseases induce a chronic, low-grade systemic inflammatory state that impairs endothelial function via the coronary microcirculation and leads to

Correspondence to: Jes-Niels Boeckel, PhD, Klinik und Poliklinik für Kardiologie, Universitätsklinikum Leipzig, Johannisallee 30, 04103 Leipzig, Germany. Email boeckel@medizin.uni-leipzig.de

Supplemental Material is available at https://www.ahajournals.org/doi/suppl/10.1161/CIRCRESAHA.125.326249.
For Sources of Funding and Disclosures, see page XXX.

Circulation Research is available at www.ahajournals.org/journal/res

Novelty and Significance

What Is Known?

- Heart failure with preserved ejection fraction (HFpEF) is strongly associated with extracardiac risk factors such as obesity, hypertension, and diabetes, which causes a chronic, low-grade systemic inflammatory state.
- Previous studies on myocardial biopsies provided results regarding inflammatory activity in HFpEF, suggesting a difference between systemic and local inflammation.

What New Information Does This Article Contribute?

- This study provides the first comprehensive, cell type–specific analysis of circulating immune cell profiles in HFpEF using single-cell and bulk RNA sequencing and reveals an inflammatory fingerprint in the HFpEF group that was significantly distinct from the heart failure with reduced ejection fraction (HFrEF) group.
- The identification of a conserved set of inflammatory and mitochondrial-associated genes in human and murine HFpEF models supports the relevance of systemic inflammation as a central pathomechanism in HFpEF.
- The beneficial effect of nitro-oleic acid in an HFpEF animal model caused by high-fat diet and L-NAME, leading to normalization of immune cell profiles and improvement of diastolic function, provides a rationale for testing a novel therapeutic approach in patients with HFpEF.

HFrEF is characterized by predominantly monocyte-mediated inflammatory activation. However, comparable immunologic mechanisms in HFpEF, an increasingly common and clinically difficult-to-treat form of heart failure, were previously unclear. This study comparatively analyzed the systemic immune cell profiles of patients with HFpEF and HFrEF. Unlike HFrEF, HFpEF did not exhibit an inflammatory response dominated by monocytes; rather, there was increased activation of natural killer cells and T lymphocytes. Similarly, metabolic activation was observed in immune cells in patients with HFpEF, indicating immunometabolic dysregulation. Importantly, nitro-oleic acid was found to attenuate pathological immune activation in an HFpEF animal model. Under nitro-oleic acid treatment, the composition and activation of immune cells largely normalized to healthy levels. This study, thus, reveals an unknown difference in immune mechanisms between HFpEF and HFrEF, providing the first indication that targeting immune metabolism could positively influence HFpEF-associated inflammatory processes. These findings pave the way for new research and therapeutic approaches. Future studies should consider HFpEF to be an independent immunologic disease process and further evaluate immunometabolic strategies, such as nitro-oleic acid, as potential therapeutic options, with the aim of improving the inadequate current treatment options for HFpEF.

Nonstandard Abbreviations and Acronyms

Ct	cycle threshold
DEG	differentially expressed gene
FBS	fetal bovine serum
HFpEF	heart failure with preserved ejection fraction
HFrEF	heart failure with reduced ejection fraction
IL	interleukin
NAMPT	nicotinamide phosphoribosyltransferase
NO_2-OA	nitro-oleic acid
NT-proBNP	N-terminal pro-B-type natriuretic peptide
PBMC	peripheral blood mononuclear cell
scRNA-seq	single-cell RNA sequencing
TNF-α	tumor necrosis factor alpha

the development of fibrosis and deterioration of diastolic function.[3]

Although previous studies on myocardial biopsies have provided evidence of inflammatory signaling in HFpEF,[4–6] more recent studies show that classical proinflammatory gene expressions (eg, *IL1B*) are not consistently elevated in the myocardium in advanced HFpEF.[7,8] This discrepancy suggests that the inflammatory processes in HFpEF are primarily systemic via circulating immune cells and do not manifest as pronounced myocardial inflammation.[1]

These findings do not refute the role of inflammation in HFpEF but rather point to its complexity, suggesting that inflammatory pathways may be spatially or temporally distinct and that some remodeling processes may be inflammation-independent under certain conditions.

These apparent discrepancies likely reflect the biological heterogeneity of HFpEF and differences in specific patient populations, disease stages, and tissues examined. Therefore, the aim of our study is to

comprehensively characterize the circulating immune cell profiles in HFpEF to gain new insights into the pathogenic mechanisms.

Here, we used single-cell RNA sequencing (scRNA-seq) technologies to analyze peripheral blood mononuclear cells (PBMCs) from patients with HFpEF, patients with HFrEF, and controls and validated the results by bulk RNA sequencing. In addition, a murine HFpEF model was analyzed to identify conserved inflammatory signatures between humans and mice and investigate the therapeutic effect of the anti-inflammatory nitro-oleic acid (NO_2-OA). The aim is to better understand the systemic immune response in HFpEF and develop potential targeted therapeutic approaches.

METHODS

Data Availability

The mouse scRNA-seq and mouse and human bulk RNA sequencing data sets shown in this publication can be accessed at the National Center for Biotechnology Information Gene Expression Omnibus with accession number GSE298197.

Patient Inclusion, Cohort 1

We conducted scRNA-seq of PBMCs from patients with HFpEF (n=6), patients with HFrEF (n=8), and control subjects (n=7) with and without obesity (body mass index: lean [<30 kg/m^2] and obese [>30 kg/m^2]). The study was approved by the local ethics committee (University of Leipzig, Germany; 008/20-ek).[5] Exclusion criteria included active smoking, autoimmune disease, or significant hematologic disease. Inclusion criteria for HFpEF were symptomatic heart failure in NYHA class ≥II, preserved left ventricular ejection fraction ≥50%, left ventricular diastolic dysfunction on echocardiography, and elevated NT-proBNP (N-terminal pro-B-type natriuretic peptide) levels (>125 pg/mL). Exclusion criteria for HFpEF were anemia, suspected storage disease, significant coronary artery disease, valvular heart disease, ICD or pacemaker, precapillary pulmonary hypertension, and a history of pericarditis. Inclusion criteria for HFrEF were clinically stable heart failure with reduced left ventricular ejection fraction (≤40%) of ischemic origin. Exclusion criteria for HFrEF included relevant valvular heart disease (moderate or greater stenosis or regurgitation), history of myocarditis, regular alcohol consumption, illicit drug use, cardiotoxic chemotherapy, or unclear pathogenesis of heart failure.

Validation Cohort, Cohort 2

Patients with HFpEF were invasively diagnosed by pressure-volume-loop analysis within the DIAGNOSE-HFpEF study (Unique identifier: NCT04688905). This study included patients with unexplained dyspnea, normal pulmonary function, and preserved ejection fraction. This study is approved by the ethics committee of Leipzig University (283/20). Patients with HFrEF were recruited from the PEDAL-HF and DIAST-CHF observational studies. PEDAL-HF (Unique identifier: NCT06656832) recruits patients with heart failure with a recent acute cardiac decompensation and follows them for 2 years. Patient enrollment occurs within 72 hours of hospitalization. The study was approved by the ethics committee of Leipzig University (242/24-ek). DIAST-CHF is a prospective observational cohort study of patients aged between 50 and 85 years with cardiovascular risk factors or heart failure.[9]

Mice Study, Cohort 3+4

Cardio metabolic syndrome was induced by a high-fat diet combined with eNOS inhibitor L-NAME.[10] ScRNA-seq was conducted from PBMCs of C57BL/6N male mice subjected to an HFpEF-inducing regimen for 15 weeks, with additional treatment of NO_2-OA for the last 4 weeks. Control mice were fed regular chow. All animal studies were approved by the local animal care committees (LANUV, Germany).[11]

For consistency in experimental conditions, only male mice were used for PBMC isolation in this study. While the efficacy of NO_2-OA has also been evaluated in female high-fat diet+L-NAME mice,[12] differences in phenotype severity precluded direct inclusion of female animals in the current PBMC analysis. For more information, please see the Major Resources Table in the Supplemental Material.

Statistical Analysis

GraphPad Prism 8 was used for statistical analysis unless otherwise stated. Normality of distributions was assessed in a standardized and consistent manner using the Shapiro-Wilk test as implemented in Prism. Comparisons of >2 groups were performed with 1-way ANOVA: paired Gaussian-distributed values were analyzed by repeated measures 1-way ANOVA, followed by the Tukey multiple comparisons test, with a single pooled variance; unpaired Gaussian-distributed values by ordinary 1-way ANOVA followed by the Tukey multiple comparisons test, with a single pooled variance; and unpaired non–Gaussian-distributed values by the Kruskal-Wallis test followed by the Dunn multiple comparisons test. $P<0.05$ was considered significant. In selected cases, $P<0.1$ is shown to indicate biological trends of potential interest for follow-up investigations. R, version 4.3, was used to identify significantly differentially expressed genes (DEGs) and GO terms. The FindMarkers function (DEGs) uses, by default, the Wilcoxon rank-sum test with Bonferroni-corrected *P* values. The TopGO package (GO analysis) uses, by default, the Fisher exact test with subsequent Benjamini and Hochberg correction. To ensure full transparency, Excel S1 in the Supplemental Material provides the statistical test used for each figure panel, the software used, and the rationale for test selection.

Single-Cell RNA Sequencing

Human PBMC Collection

Control and patient blood was collected in EDTA monovettes and processed immediately. Specifically, blood was diluted in PBS (Thermo Fisher, 10010023) and layered onto Histopaque-1077 (Sigma-Aldrich, 10771). Tubes were centrifuged for 30 minutes at RT, 800*g*, brake, and speed-up 1, and PBMCs were collected from the interphase between Histopaque-1077 and plasma. PBMCs were washed 5× with PBS, and counted and frozen at −80°C in a 1:1 mixture of resuspension (40% fetal bovine serum [FBS] in RPMI) and 2× freezing medium (30% dimethyl sulfoxide in RPMI containing

40% FBS) according to the 10× Genomics-demonstrated protocol CG00039. The next day, PBMCs were transferred to liquid nitrogen for long-term storage.

Mouse PBMC Collection

Mouse blood was collected into syringes preloaded with 10 µL of 0.5-M EDTA (pH, 8.0) to prevent coagulation. After gentle mixing, the blood was transferred to Eppendorf tubes, and plasma was separated by centrifugation at 500*g* for 5 minutes. The remaining blood was diluted in PBS (1:3 dilution) and layered over Ficoll (Merck, GE17-5446-02). Samples were centrifuged at 400*g* for 30 minutes at RT without brake. PBMCs were collected from the interphase, washed in PBS supplemented with 0.3-mmol/L EDTA and 2% FBS, and pelleted at 400*g* for 8 minutes. Red blood cells were lysed with erythrocyte lysis buffer (10 minutes, RT; 0.83% [w/v] NH_4Cl; 10-mmol/L Hepes-NaOH; pH, 7.4), followed by centrifugation. Cells were resuspended in 100-µL PBS and counted using Trypan Blue. PBMCs were frozen in a 1:1 mixture of resuspension medium (40% FBS in RPMI) and 2× freezing medium (30% dimethyl sulfoxide in RPMI containing 40% FBS), transferred to cryovials, and initially stored at −80 °C using a controlled-rate freezing container before long-term storage in liquid nitrogen.

Single-Cell Preparation and Barcoding

PBMCs were thawed according to the 10× Genomics-demonstrated protocol CG00039, and a cell concentration of 700 to 1200 PBMCs per µL of PBS+0.04% BSA was set. Chromium Next GEM Single Cell 3′ GEM, Library & Gel Bead Kit v3.1 (10× Genomics, PN-1000128, Chip G: 1000127) was used to generate GEMs, reverse transcribe RNA, and amplify cDNA according to the manufacturer's instructions. Targeted cell recovery was 10 000 cells.

Library Construction and Sequencing

After cleanup (step 2.3), 2 µL of the cDNA was used for quality control on the Agilent fragment analyzer (DNF-473 Standard Sensitivity NGS Fragment Kit). In addition, 10 µL of the cDNA was used as input for step 3 of the Chromium Next GEM Single Cell 3′ Reagent Kit to perform fragmentation, end repair, A-tailing, and adapter ligation. The obligatory polymerase chain reaction of the protocol was performed with 13 cycles. The finished library was monitored again using the fragment analyzer, and the DNF-473 Standard Sensitivity NGS Fragment Kit. Equimolar amounts of each sample were plexed at 1.25 nmol/L. Sequencing was performed as paired-end 2×150 bp (S4-Flowcell) on a NovaSeq 6000 (Illumina). Fastq files generated by bcl2fastq (version 2.20.0.422) were processed with cellranger count against the human hg38 reference or the mouse mm39 reference. The mean sequencing depth was ≈227.24±26.18 (SEM) million reads per sample in the human single-cell sequencing data set and ≈582.42±24.91 (SEM) million reads per sample in the murine single-cell sequencing data set.

Data Analysis: Cell Type Annotation

Cell Ranger output was used to create Seurat objects (satijalab.org) in RStudio. Possible dead cells (percentage of mitochondrial genes >10%) and empty droplets (nFeature_RNA <200) were filtered out, and Seurat objects were normalized using NormalizeData. Normalized data sets were integrated, and the main cell types, monocytes, T cells, B cells, natural killer cells, platelets, red blood cells, and progenitor cells, were assigned to the clusters, taking into account the expression of established markers. For the human data set, results from the SingleR tool[13] with the reference data sets, HumanPrimaryCellAtlasData, BlueprintEncodeData, NovershternHematopoieticData, DatabaseImmuneCellExpressionData, and MonacoImmuneData from the package celldex, were also taken into account. A subset of each data set with an equal number of cells per condition was created for comparison plots, such as FeaturePlots.

Next-Generation Bulk RNA Sequencing

Quality control and quantification of the isolated RNA were performed using the Fragment Analyzer 5200 (Agilent) using the High Sensitivity RNA quantification kit and Fragment Analyzer Controller Software (Agilent, version 3.1.0.12). Random primed library preparation was started with 150 ng of total RNA using the Watchmaker RNA library prep kit with Polaris depletion (Watchmaker Genomics) according to the instructions of the manufacturer. The barcoded libraries were purified and quantified using Qubit Fluorometric Quantification (Thermo Fisher Scientific). The size distribution of the library DNA was analyzed using the Fragment Analyzer 5200 (Agilent). Sequencing of 2×150 bp was performed with an Illumina NovaSeq 6000 sequencer (Illumina, San Diego, CA). After demultiplexing with the bcl2fastq software (Illumina, version 2.20), the fastq files underwent trimming and adapter removal using Trim Galore. Read mapping was performed against the respective reference genome (human hg38/mouse mm39) using *Hisat2*. Gene expression quantification was achieved by read counting using FeatureCounts (R package). The resulting counts were then converted to transcripts per million or trimmed mean of M values for normalization in R.

The 42 human whole blood samples from cohort 2 were sequenced with an average of 40.20±0.51 (SEM) million reads per sample. The 18 cell culture PBMC samples were sequenced with an average of 48.33±0.50 (SEM) million reads per sample. The 16 mouse PBMC samples from cohort 4 were sequenced with an average of 82.54±7.07 (SEM) million reads per sample.

Isolation of PBMCs

PBMCs were isolated from buffy coats of healthy blood donors (ethical vote 272-12-13082012, University Leipzig) by density gradient centrifugation. In particular, blood was diluted in PBS (Thermo Fisher, 10010023) containing 0.3-mmol/L EDTA and layered onto Ficoll Paque (Cytiva, 17144003). Tubes were centrifuged for 20 minutes at RT, 2030 rpm, and brake 4, and PBMCs were collected from the interphase between Ficoll Paque and plasma. PBMCs were washed multiple times with PBS containing 0.3-mmol/L EDTA and 0.2% BSA and used for further experiments.

Treatment of PBMCs

Human primary PBMCs or THP1 cells (human monocytic cell line used for immunofluorescence; DSMZ, ACC 16) were seeded in cell culture plates in RPMI-1640 medium (Merck, R8758) supplemented with 10% FBS (Gibco, 10500064). NO_2-OA (50:50 mix of [E]-9- and 10-nitrooctadec-9-enoic acid) was added for a final concentration of 1 or 3 µmol/L.

After 2.5 hours pre-treatment, PBMCs were treated for an additional 15 minutes to 24 hours and THP1 cells for an additional 15 minutes with the following cytokines and concentrations: IL (interleukin)-1β (10 ng/mL; Sigma-Aldrich, H6291-10UG), TNF-α (tumor necrosis factor alpha; final concentration: 10 ng/mL; Peprotech, 300-01A), and IL-6 (10 ng/mL; R&D Systems, 206-IL-050/CF). For quantitative polymerase chain reaction and bulk RNA-seq, PBMCs were harvested after 4.5-hour cytokine treatment for the time course after 1-, 3-, 6-, 14-, 19-, and 24-hour IL-1β treatments and for immunoblotting and immunofluorescence after 15-minute IL-1β treatment.

RNA Isolation and Reverse Transcription

RNA was purified from cells/whole blood using the miRNeasy kit (Qiagen, 217004) according to the manufacturer's instructions with additional DNase (Qiagen, 79254) digestion. RNA was reverse transcribed to cDNA (1× buffer, 10-mmol/L DTT; both: Thermo Fisher, 18057018), 5-µmol/L random hexamer primers (Thermo Fisher, S0142), 0.25-mmol/L dNTPs (Thermo Fisher, 18427013), 1-U/µL RiboLock RNase inhibitor (Thermo Fisher, EO0381), and 2.5-U/µL M-MLV reverse transcriptase (Thermo Fisher, 28025013), as described recently.[14]

Quantitative Real-Time Polymerase Chain Reaction

Quantitative polymerase chain reaction was performed on a StepOne real-time polymerase chain reaction system (Thermo Fisher) using SYBR green master mix (Thermo Fisher, A25778) according to the manufacturer's instructions. Cycle threshold (Ct) values were normalized to the corresponding RPLP0 Ct values (ΔCt), and relative expression levels were calculated using the $2^{-\Delta Ct}$ method described recently.[15] The following primers were used: hRPLP0-f: TCGACAATGGCAGCATCTAC, hRPLP0-r: ATCCGTCTCCACAGACAAGG, hIL1B-f: CACG AATGCACCTGTACGATCA, and hIL1B-r: GTTGCTCCATATCC TGTCCCT.

Immunoblotting

PBMCs were lysed for 30 minutes on ice in RIPA buffer containing 1X HALT protease/phosphatase inhibitor cocktail (Thermo Scientific, 78429). The concentration of isolated proteins was measured using a BCA assay, and equal amounts of total protein were loaded onto 4% to 15% Mini-PROTEAN TGX precast protein gel (Bio-Rad, 4561084). SDS-PAGE was performed, and proteins were blotted onto a 0.45-µm nitrocellulose membrane (Bio-Rad, United States). The membrane was blocked in 5% nonfat dry milk and incubated with antibodies directed against phospho-NF-κB (Ser536; 1:1000 in 5% BSA, stock concentration: 57 µg/mL; cell signaling, 3033S), IL-1β (1:1000 in 5% BSA, stock concentration: 1 mg/mL; antibodies, A87561), and GAPDH (1:10 000 in 5% nonfat dry milk, stock concentration 200 µg/mL; Santa Cruz, sc-47724), respectively. GAPDH, used as the internal loading control, was always detected on the same membrane as the respective target protein to ensure reliable normalization in accordance with current best practices. Polyclonal goat anti-rabbit immunoglobulins/HRP (1:1000 in 5% nonfat dry milk; Agilent Dako, P0448) and polyclonal goat anti-mouse immunoglobulins/HRP (1:1000 in 5% nonfat dry milk; Agilent Dako, P0447) were used as secondary antibodies. For membranes probed sequentially with multiple primary antibodies, a stripping step was performed before reprobing. Membranes were incubated in stripping buffer (Roth, 3337.2) for 30 minutes at RT on a shaker, followed by 3 washes with TBST. After blocking again for 1 hour in 5% nonfat dry milk at RT, membranes were washed 3× in TBST and then reprobed with GAPDH antibody. For more information on the antibodies used, please see the Major Resources Table in the Supplemental Material.

Immunofluorescence

THP1 cells were adhered to glass coverslips by gravity sedimentation.[16] Briefly, cells were pelleted by centrifugation at 250*g* for 5 minutes, the supernatant was aspirated, and the pellet was resuspended in PBS at a concentration of 1×10^6 cells/mL; 1 mL of the cell suspension was added to each well of a 12-well culture plate containing a glass coverslip. Coverslips were kept submerged using a pipette tip, and cells were allowed to settle and adhere at RT for 30 minutes. Nonadherent cells were gently removed by aspirating the PBS. Adherent cells were fixed with 500 µL of 4% formaldehyde (Roth, P087.6) for 10 minutes at RT, followed by a 5-minute PBS wash. Permeabilization was performed using 500 µL of 0.5% Triton X-100 (Sigma-Aldrich, T8787-100 mL) for 10 minutes and then, cells were washed again with PBS. Cells were blocked with donkey serum (Sigma-Aldrich, D9663) for 30 minutes and subsequently incubated with 250-µL primary antibody phospho-NF-κB (Ser536; 1:800, stock concentration: 57 µg/mL; cell signaling, 3033S) diluted in 1% BSA (Thermo Fisher, 15260037) overnight at 4 °C. After 3 PBS washes (5 minutes each), cells were incubated with 250-µL Donkey anti-Rabbit IgG (H+L) Highly Cross-Adsorbed Secondary Antibody, Alexa Fluor 488 (1:200, stock concentration: 2 mg/mL; Thermo Fisher, A-21206) in 1% BSA for 1 hours at RT, protected from light. Following 3 additional PBS washes, antibody acti-stain 555 phalloidin (1:140, stock concentration: 14 µmol/L; cytoskeleton, PHDH1) was added for 30 minutes. Following another 3 PBS washes, nuclei were counterstained with Hoechst dye (1:200, stock concentration: 200 µg/mL; Biomol, ICT-639) for 10 minutes and washed twice with PBS. Coverslips were mounted cell-side down onto microscope slides with Fluorescence Mounting Medium (Agilent, S302380-2). Images were acquired using a 63× oil immersion objective.

Illustrations

Drawn elements from Servier Medical Art by Servier licensed under a Creative Commons Attribution 3.0 Unported License (https://creativecommons.org/licenses/by/3.0/) were used in original or modified form to create the illustrations.

RESULTS

Comparing the Immune Cell Signatures of HFpEF, HFrEF, and Obesity in Humans

To characterize the peripheral immune cell populations in patients with HFpEF, scRNA-seq of human immune cells obtained from patients with HFpEF (n=6), patients with HFrEF (n=8), and controls (n=7) with and without

obesity was conducted (cohort 1, scRNA-seq; Table 1). Data integration from the resulting 158 802 cells identified 18 distinct clusters (Figure 1A). Cell types were assigned to these clusters on the basis of established immune cell markers[17] (eg, *CD14* for monocytes, *CD79A* for B cells, and *CD3E* for T cells), as well as results from the SingleR tool[13] (Figure 1B). The resulting cell type annotations revealed an elevated monocyte/T-cell ratio in HFrEF[17] but not in patients with HFpEF. The percentages of both proinflammatory T helper 17 and anti-inflammatory Treg cells were only reduced in HFrEF (Figure 1C and 1D). Immune cell type–specific analysis revealed that natural killer cells and T cells showed an activated transcriptional profile in patients with HFrEF and HFpEF (Figure 1E). Significantly upregulated DEGs were identified for individuals with obesity (n_{DEG}=531), HFrEF (n_{DEG}=605), and HFpEF (n_{DEG}=240). The 3 diseases, obesity, HFpEF, and HFrEF, show similarities although these are greater for HFpEF and HFrEF than for obesity with HFpEF and HFrEF, respectively (Figure 1F and 1G). Analyzing the inflammatory profile revealed that obesity was characterized by an increase in *IL1A*, *IL6*, and *IL1B*, and lean and obese HFrEF by an increase in *IL1B*, *IL8* (*CXCL8*), *CXCL2*, and *TNF*. Lean HFpEF showed an increase in MCP1 (*CCL2*), and obese HFpEF showed an increase in *TNF* (Figure 1H). To analyze these findings in a larger cohort and to investigate whether the observed differences between HFpEF and HFrEF may be driven by the ischemic cause of the patients with HFrEF, we performed bulk RNA sequencing of whole blood samples from patients with ischemic (n=5) and nonischemic (n=11) HFrEF, as well as HFpEF (n=18; cohort 2, bulk RNA-seq; Table 2; Figure 1I). An analysis of the activated high-level orchestrated signaling pathways revealed disease-specific profiles. Complement system activation was prominent in obesity and HFrEF but absent in HFpEF (cohort 1, scRNA-seq; Figure 1J). In contrast, HFpEF was characterized by increased mitochondrial activity, reflected by upregulation of genes such as *ATP5ME*, *ATP5F1E*, *UQCRQ*, and *NDUFB*, natural killer cell-specific regulation, and coronary vascular morphogenesis (Figure 1G and 1J).

Moreover, HFpEF-regulated genes exhibited partially immune cell type–specific expression patterns (cohort 1, scRNA-seq; Figure 1K).

Comparing the Immune Cell Signatures of HFpEF in Humans and Mice

To identify conserved immune response genes across species and assess the effect of NO_2-OA therapy on immune cells, we performed single-cell sequencing and bulk RNA sequencing of PBMCs of an HFpEF mouse model (cohort 3+4; Figure 2A). Cardio metabolic syndrome was induced in C57BL/6N mice by a high-fat diet combined with eNOS inhibitor L-NAME for 15 weeks.[10] A subgroup of the mice subjected to the HFpEF-inducing regimen was additionally treated with NO_2-OA for the last 4 weeks. Control mice were fed regular chow. The HFpEF phenotype was characterized by preserved left ventricular ejection fraction (Figure 2B) with a concomitant increased left atrial area (Figure 2C) and an increased ratio of early diastolic velocity of mitral inflow to early diastolic velocity of the mitral annulus (Figure 2D), whereas treatment with NO_2-OA improved diastolic dysfunction in HFpEF mice (Figure 2B through 2E).[11] ScRNA-seq of PBMCs and subsequent cell type clustering from the resulting 57 097 cells identified 16 distinct clusters (cohort 3, scRNA-seq; Figure 2F). HFpEF mice were analyzed for changes in the proportion of immune cells compared with control mice (cohort 3, scRNA-seq; Figure 2G). Analysis of the inflammatory signatures in immune cells of HFpEF mice showed an increase in *Il1a*, *Il6*, *Il1b*, and Mcp1 (*Ccl2*; Figure 2H), which was additionally analyzed by bulk RNA sequencing of PBMCs of more mice (n=16; cohort 3, bulk RNA-seq; Figure 2I). The NO_2-OA–treated HFpEF group showed partial normalization of this imbalance of immune cell types and inflammatory expression in both the screening cohort (cohort 3, scRNA-seq) and the validation cohort (cohort 4, bulk RNA-seq), suggesting that targeted anti-inflammatory approaches may modulate systemic immune profiles in this animal model of HFpEF (Figure 2G through 2I). A comparison of human and murine

Table 1. Baseline Characteristics of Cohort 1

	Control		HFrEF		HFpEF	
Characteristics	Lean	Obese	Lean	Obese	Lean	Obese
Age, y	68.6±2.3	68.5±1.5	70.6±3.1	69.7±1.9	78.7±3.0	72.7±4.4
Sex, f/m	1/4	1/1	0/2	0/6	2/1	2/1
BMI, kg/m²	24.7±1.3	39.2±6.5	23.6±2.1	35.0±2.2	26.3±1.1	40.5±3.7
LVEF, %	59.6±1.8	64.0±0.0	27.5±0.5	37.8±1.5	58.0±4.0	63.0±0.6
NT-proBNP, ng/L	69.8±15.8	110.4±20.7	2603.5±572.5	1599.7±1190.3	1038.7±342.3	432.7±50.0

Data are presented as n (%) or mean±SEM. For each parameter, all patients have been accounted for unless otherwise declared (n=x). If NT-proBNP was below the detection limit (<50 ng/dL), it was set to 50 ng/dL. BMI indicates body mass index; f, female; HFpEF, heart failure with preserved ejection fraction; HFrEF, heart failure with reduced ejection fraction; LVEF, left ventricular ejection fraction; m, male; and NT-proBNP, N-terminal pro-B-type natriuretic peptide.

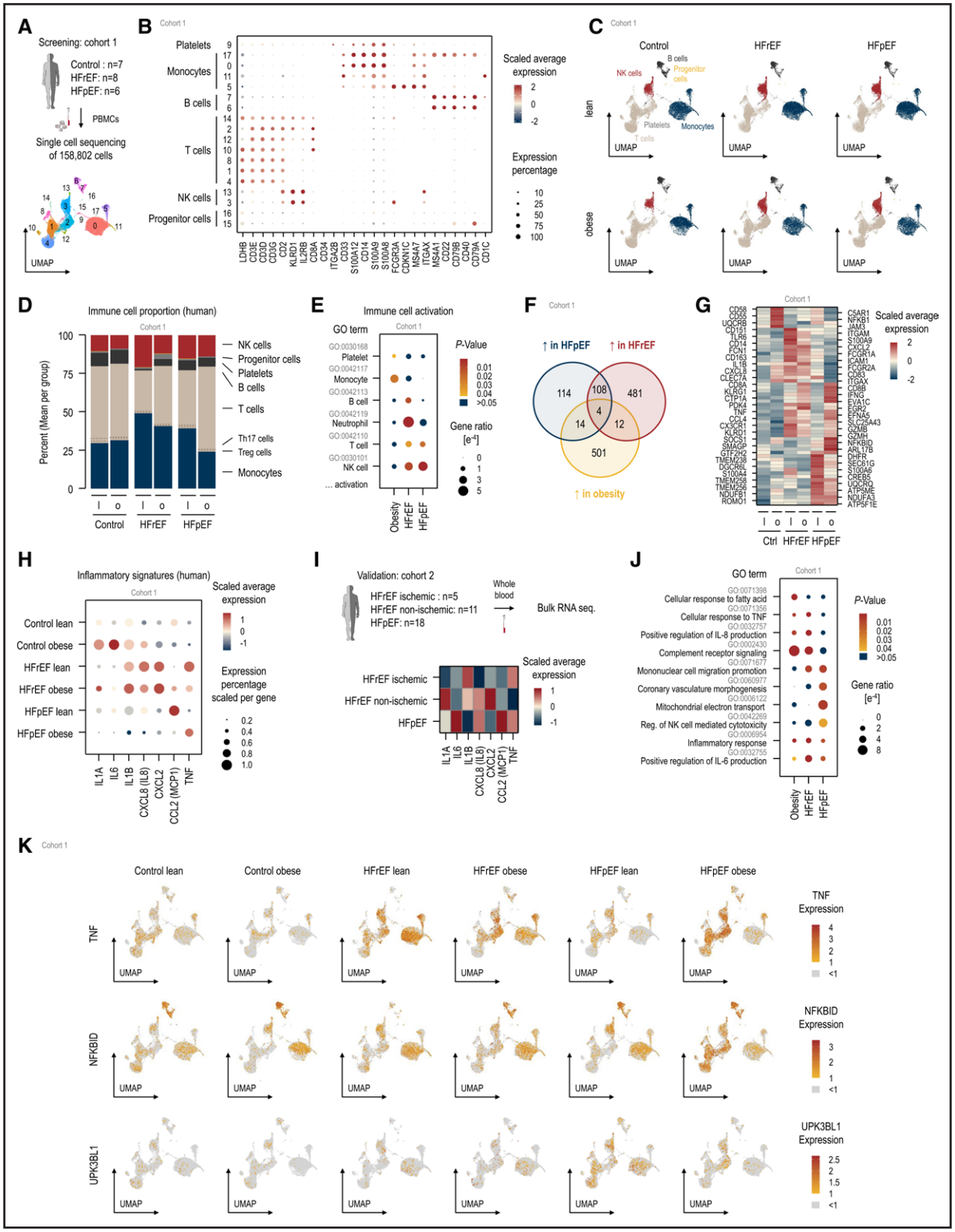

Figure 1. Comparing the immune cell signatures of heart failure with preserved ejection fraction (HFpEF), heart failure with reduced ejection fraction (HFrEF), and obesity in humans.

A, Peripheral blood mononuclear cells (PBMCs) were isolated from blood samples drawn from controls (Ctrls; n=7) and patients with heart failure (HF) with reduced (n=8) or preserved (n=6) ejection fraction and then subjected to single-cell RNA sequencing (scRNA-seq; cohort 1). The uniform manifold approximation and projection (UMAP) plot shows the 18 clusters of PBMCs identified by FindClusters. **B**, Different immune cell markers were used for annotation of the clusters to the cell types: platelets, monocytes, B cells, T cells, natural killer (NK) cells, and progenitor cells (Ctrl, n=7; HFrEF: n=8; and HFpEF: n=6). A dot plot shows the percentage of cells expressing the gene and the scaled average (*Continued*)

HFpEF-regulated DEGs from scRNA-seq using the OrthoIntegrate tool showed the percentage of species-specific and common orthologous DEGs per immune cell type (cohort 1 versus cohort 3, both scRNA-seq; Figure 2J). An analysis of the immune cell type–specific expression density of the identified ortholog-regulated DEGs in mice and humans revealed marked differences in primary cell of origin expression despite orthologous disease regulation, suggesting HFpEF-specific conservation of DEGs but in other immune cell types in humans and mice (cohort 1 versus cohort 3, both scRNA-seq; Figure 2K). Treatment with NO_2-OA reduced the expression of selected orthologous DEGs that were simultaneously induced in human and murine HFpEF. Consistent with the literature, NO_2-OA regulated ortholog-regulated genes involved in mitochondrial activity, such as *NDUFA3*, *UQCRQ*, and *UQCR11*, but also counteracted the elevation of genes known to be associated with heart failure, such as RHOC (cohort 1 versus cohort 3, both scRNA-seq; Figure 2L and 2M).[11] Bulk RNA sequencing data were used to validate the single-cell sequencing data of human and mouse PBMCs (cohort 2 versus cohort 4, both bulk RNA-seq; Figure 2N and 2O).

NO_2-OA Treatment Reduces the Inflammatory Response of Human Immune Cells

Next, we investigated whether the anti-inflammatory effect of NO_2-OA treatment in mice is transferable to humans (Figure 3A). Therefore, PBMCs from healthy human donors were pretreated with increasing concentrations of NO_2-OA before induction of inflammation using different cytokines. Pretreatment with increasing concentrations of NO_2-OA abolished the induction of inflammation by proinflammatory cytokines (Figure 3B through H). An analysis of the time-dependent effect of NO_2-OA after inflammation induction by IL-1β treatment showed a strong anti-inflammatory effect on the induction of *IL1B* mRNA expression already after 4.5 hours (Figure 3C). Subsequent analysis of the immune cell transcriptome using bulk RNA-seq showed a broad and robust anti-inflammatory response with increasing NO_2-OA concentrations (Figure 3D; Figure S1A through S1D). Further validation of the sequencing data for selected genes showed effects both in the area of classical inflammation such as *IL1B* or *CASP1*, which mediates IL-1β cytokine maturation, and in markers of metabolic pathology such as *INSIG1*, which plays a critical role in the regulation of cholesterol concentration in cells, or *OLR1*, the receptor for oxidized LDL (Figure 3E through 3H). Furthermore, we analyzed a possible influence on the phosphorylation of NF-κB and on the cytokine maturation of IL-1β in human immune cells after pretreatment with NO_2-OA and subsequent inflammation induction by IL-1β (Figure 3I and 3J). In the next step, DEGs were identified in immune cells that were orthologously regulated by NO_2-OA in humans and mice. This was done by comparing genes that were downregulated in human immune cells, which were pretreated with NO_2-OA prior to inflammation induction compared with vehicle-pretreated, inflammation-activated immune cells with genes that were downregulated in mouse immune cells after NO_2-OA treatment in the HFpEF model (cell culture+cohort 4, both bulk RNA-seq; Figure 3K through 3M). Among the orthologous-regulated genes, we found many genes predominantly expressed in monocytes, such as CD14, C3AR1, DAPK1, and LYZ. Finally, the orthologue-regulated DEGs were analyzed for validation in the scRNA-seq data set of the mouse HFpEF model treated with NO_2-OA (cohort 3, scRNA-seq; Figure 3N).

Figure 1 Continued. expression level. Scaled average expression refers to *Z* score normalized gene expression values. This standardization centers the values on 0 and scales the variance to 1. **C**, UMAP plots show the final annotation of single-cell clusters to immune cell types in PBMCs from Ctrls (n=7) and patients with heart failure (HFrEF: n=8; HFpEF: n=6) separated by body mass index (BMI; lean [l]: <30 kg/m^2; obese [o]: >30 kg/m^2; cohort 1); 12900 randomly selected cells are shown in each plot for comparability. **D**, Stacked bar plots show percentages of the annotated immune cell types as mean per group (cohort 1). **E**, The dot plot gives information about cell activation in each disease. Using FindMarkers (logfc.threshold=0.5, min.pct=0.05, and only.pos=TRUE), differentially expressed genes (DEGs) between Ctrl o and Ctrl l, HFrEF (l+o), and Ctrl (l+o), as well as HFpEF (l+o) and Ctrl (l+o), were identified (cohort 1). Significantly upregulated DEGs (Wilcoxon rank-sum test, Bonferroni-corrected *P*<0.05) were then subjected to separate GO analyses using TopGO. A gene ratio was calculated for each GO term by dividing the number of significantly regulated genes by the total pathway genes and then normalized by the number of genes used in each GO analysis (obesity: 531; HFrEF: 605; and HFpEF: 240). The dot plot shows selected GO terms, gene ratio (dot size), and *P* value (dot color). Nonsignificant GO terms were colored blue. Significant GO pathways were identified using the Fisher exact test in TopGO, followed by Benjamini and Hochberg correction. **F**, Venn diagram shows the number of significantly upregulated genes (see text dot plot in **E**) in each disease and overlaps (cohort 1). **G**, Heat map and (**H**) dot plot show scaled average expression (color) of selected genes (cohort 1). Scaled average expression refers to *Z* score normalized gene expression values. This standardization centers the values on 0 and scales the variance to 1. Dot size indicates the percentage of cells expressing each gene scaled by the maximal percentage per gene. **I**, Bulk RNA sequencing was performed of RNA isolated from whole blood of patients with HFrEF (ischemic, n=5; nonischemic: n=11) and HFpEF (n=18; cohort 2). Heat map shows scaled average expression (color) of genes shown in **H**. Scaled average expression refers to *Z* score normalized gene expression values. This standardization centers the values on 0 and scales the variance to 1. **J**, The dot plot shows selected GO terms found as described in **E** (dot plot; cohort 1), gene ratio (dot size), and *P* value (dot color). Nonsignificant GO terms were colored blue. **K**, Feature plots showing *TNF*, *NFKBID*, and *UPK3BL1* expressions in PBMCs from Ctrls (n=7) and patients with heart failure (HFrEF: n=8; HFpEF: n=6) separated by BMI (l: <30 kg/m^2; o: >30 kg/m^2; cohort 1); 12900 randomly selected cells are shown in each plot for comparability. Cells were sorted so that those with higher expression levels are displayed on top. Cells expressing the gene below the na_cutoff=1 threshold or not at all are shown in gray. **A** and **I** were drawn in part using images from Servier Medical Art. Servier Medical Art by Servier is licensed under a Creative Commons Attribution 3.0 Unported License (https://creativecommons.org/licenses/by/3.0/).

Table 2. Baseline Characteristics of Cohort 2

Characteristics	Control	HFrEF		HFpEF
		Ischemic	Nonischemic	
Age, y	67.25±1.94	77.60±1.89	64.41±5.07	63.28±2.25
Sex, f/m	5/3	1/4	4/7	10/8
BMI, kg/m^2	29.37±3.06	24.96±2.06	27.58±2.16	29.61±1.12
LVEF, %	63.83±1.42 (n=6)	38.20±2.75	33.91±2.07	59.98±0.92
NT-proBNP, ng/L	78.50±10.20	10096.66±5533.50	3247.21±1132.05 (n=10)	243.48±59.13
Characteristics	Control		HFpEF	
	Lean	Obese	Lean	Obese
Age, y	67.50±3.38	67.00±2.48	59.44±3.22	67.11±2.74
Sex, f/m	2/2	3/1	5/4	5/4
BMI, kg/m^2	22.40±1.15	36.33±3.15	25.77±0.71	33.46±1.06
LVEF, %	64.00±0.00 (n=2)	63.75±2.25	61.44±1.47	58.51±0.94
NT-proBNP, ng/L	59.00±10.48	98.00±11.05	163.31±40.59	323.66±107.74

Data are presented as n (%) or mean±SEM. For each parameter, all patients have been accounted for unless otherwise declared (n=x). If NT-proBNP was below the detection limit (<50 ng/dL), it was set to 50 ng/dL. BMI indicates body mass index; f, female; HFpEF, heart failure with preserved ejection fraction; HFrEF, heart failure with reduced ejection fraction; LVEF, left ventricular ejection fraction; m, male; and NT-proBNP, N-terminal pro-B-type natriuretic peptide.

Validation of Identified DEGs in a Human HFpEF Cohort

In the next step, the component of obesity-dependent regulation in the setting of HFpEF was investigated in more detail by reanalyzing the human scRNA-seq data (cohort 1, scRNA-seq) to identify DEGs between obese or lean HFrEF, obese or lean HFpEF, and individuals with obesity compared with lean controls (Figure 4A). Lean HFrEF and individuals with obesity had the highest number of independently regulated DEGs. Lean patients with HFrEF and patients with obesity with HFrEF showed the greatest overlap of DEGs. A comparison of the human and mouse scRNA-seq data showed mostly similar regulation of DEGs specifically upregulated in HFpEF lean, HFpEF obese, or all patients with HFpEF in both species (cohort 1+3, both scRNA-seq; Figure 4B through 4D). However, not all genes, whose HFpEF-specific regulation was subsequently validated in the bulk sequencing data set of human whole blood (cohort 2, bulk RNA-seq; Figure 4E and 4F), showed upregulation in the HFpEF mouse model.

DISCUSSION

Our integrated transcriptomic analysis of human and murine HFpEF immune cells reveals selective systemic upregulation of proinflammatory cytokines (eg, *CCL2* and *TNF*) and dysregulation of metabolic and mitochondrial-related gene expression that differentiates HFpEF from HFrEF in the patient samples analyzed. We further demonstrate that treatment with the electrophilic fatty acid NO_2-OA can modulate these pathological immune and metabolic profiles, attenuating inflammation and improving mitochondrial-related pathways. Together, these findings underscore the pivotal role of immunometabolic interplay in HFpEF pathogenesis and highlight a potential novel therapeutic strategy to target this interplay.

Chronic low-grade inflammation emerges as a unifying mechanism linking HFpEF with its common comorbidities. Many HFpEF risk factors, obesity, type 2 diabetes, hypertension, aging, and renal dysfunction, are associated with persistent, systemic inflammation.[18] The influential comorbidity-inflammation paradigm of HFpEF postulates that these comorbid conditions drive systemic inflammatory signaling, which, in turn, causes endothelial dysfunction, reduced NO-cGMP signaling, titin hypophosphorylation, and ultimately diastolic dysfunction.[1,18] Consistently, substantial evidence indicates that circulating proinflammatory cytokines (eg, IL-6 and TNF-α) are elevated in patients with HFpEF,[19] and higher comorbidity burden correlates with increased inflammatory biomarkers such as C-reactive protein.[20–22] This state of combined metabolic stress and inflammation, often termed metaflammation, is believed to promote adverse cardiac remodeling in HFpEF.

Notably, our findings help clarify apparent discrepancies in the field regarding myocardial versus systemic inflammation in HFpEF. While earlier myocardial biopsy studies of advanced HFpEF reported a primarily profibrotic gene signature with little to no upregulation of inflammatory genes,[7] this does not necessarily contradict the concept of an inflammatory HFpEF phenotype. In fact, immune cell infiltration and activation can be present in HFpEF hearts even if bulk tissue mRNA profiles appear inert.[7] Immunohistological analyses have documented increased numbers of macrophages and

ORIGINAL RESEARCH

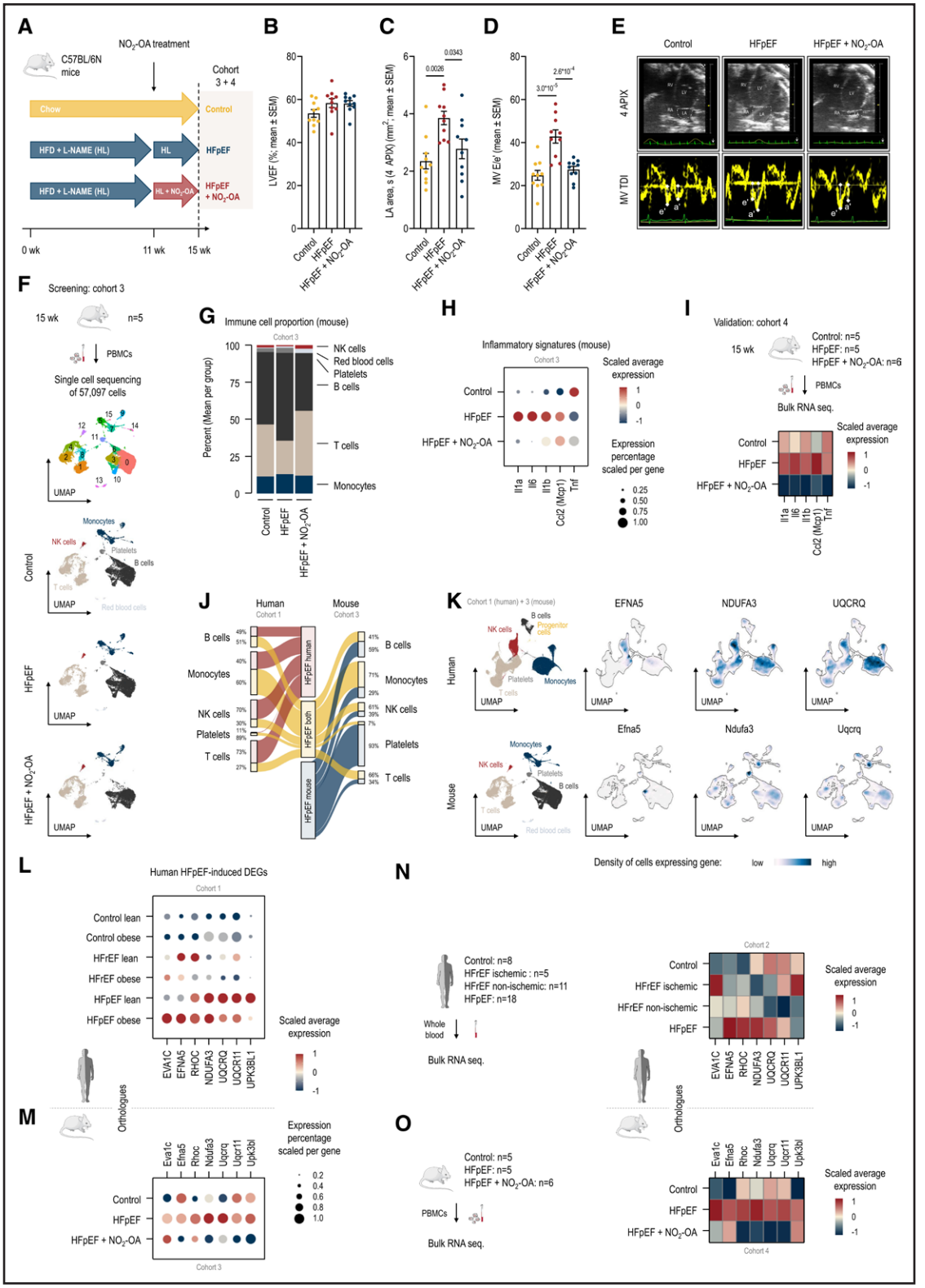

Figure 2. Comparing the immune cell signatures of heart failure with preserved ejection fraction (HFpEF) in humans and mice. **A**, C57BL/6N mice were fed either a standard (chow) or a high-fat diet (HFD; 60% fat, 20% protein, and 20% carbohydrates). HFD animals additionally received the eNOS inhibitor L-NAME via drinking water (0.5 g/L). After 11 weeks, HFD+L-NAME animals were treated for 4 weeks with vehicle or nitro-oleic acid (NO_2-OA; 50:50 mix of (E)-9- and 10-nitrooctadec-9-enoic acid) via osmotic minipumps[3] (cohorts 3+4). For simplicity, chow-fed mice will be referred to as controls, mice subjected to the HFpEF-inducing regimen as HFpEF and those receiving the HFpEF-inducing regimen plus NO_2-OA treatment as HFpEF+NO_2-OA. **B**, Left ventricular ejection fraction (LVEF), (**C**) left atrial (LA) area, and (**D**) ratio of early diastolic mitral inflow velocity to early diastolic mitral annulus velocity (MV E/e´) are shown for control (n=10), (*Continued*)

T lymphocytes in HFpEF myocardium,[4,5] along with an imbalance favoring proinflammatory T helper 17 cells over anti-inflammatory regulatory T cells.[23] Such compartmentalized inflammation may be missed in small biopsy samples or late-stage disease.[6] Our blood-based analyses captured robust immune activation, underscoring that the systemic compartment in HFpEF carries a significant inflammatory signal, even when some studies found that myocardial tissue changes in HFpEF seem dominated by fibrosis, while others demonstrated strong inflammatory activation of the coronary endothelium.[4,7] These results affirm the importance of assessing inflammation across multiple compartments and suggest that circulating immune cells can serve as sensitive sentinels of HFpEF-related inflammation, supporting the relevance of interorgan immune cross talk in HFpEF.[24] These systemic immune cell signatures could reflect myocardial processes such as activation of cardiac-resident immune cells, inflammation in adipose tissue, or microvascular immune activation or metaflammatory involvement of the liver. The activation of the immune cells could be the result of tissue-based inflammation and triggering the inflammation itself or even both. Although direct tissue analysis was not performed in this study, previous work suggests close communication between systemic immune activity and cardiac remodeling processes.

Future studies should also examine epicardial and perivascular adipose tissues in particular, as these tissues are known sources of proinflammatory signals and may contribute to myocardial dysfunction in HFpEF via paracrine mechanisms.[25,26] Our comparative analysis also illuminates how the HFpEF's immunometabolic profile of the patients with HFpEF analyzed in this study diverges from that of the patients with HFrEF. Both here analyzed patients' groups, HFpEF and HFrEF, exhibit immune activation, but the triggers and patterns differ. HFpEF is often a consequence of metabolic comorbidities, leading to a milieu of oxidative stress and low-grade inflammation (eg, from inflamed adipose tissue) rather than the postinfarct inflammatory burst typical of ischemic HFrEF. Supporting this distinction, a recent proteomic study found that although many circulating proteins are commonly dysregulated in both conditions, a subset of pathways, particularly those related to cell proliferation and fate commitment, differs significantly between HFpEF and HFrEF.[27] For instance, the profibrotic factor SLITRK6 and neural protein NELL2 were downregulated only in HFpEF, whereas the enzyme NAMPT (nicotinamide phosphoribosyltransferase), a mediator of inflammation and metabolism, was elevated in HFrEF (likely reflecting ischemic stress).[27] These observations reinforce that HFpEF is pathophysiologically distinct, characterized by a more complex interplay of systemic metabolic inflammation, as opposed to the more acute injury-driven inflammation in HFrEF. Our data extend this concept by showing unique gene expression signatures in HFpEF immune cells (eg, upregulation of inflammatory and stress-response pathways) that are not shared

Figure 2 Continued. HFpEF (n=10), and HFpEF+NO_2-OA (n=10) mice. Bar graphs are presented as mean±SEM (**B**–**D**: ordinary 1-way ANOVA with the Tukey multiple comparisons test, with a single pooled variance). **E**, Representative high-frequency ultrasound images of 4-chamber B-mode (4 APIX; **top**) to access LA area (marked area) at end systole (white arrow) and left ventricular (LV) tissue Doppler imaging (MV TDI; **bottom**) at mitral annulus to assess diastolic function. **F**, From a subset of mice shown in **A** (cohort 3; n=5), peripheral blood mononuclear cells (PBMCs) were isolated from blood samples and subjected to single-cell RNA sequencing (scRNA-seq). Uniform manifold approximation and projection (UMAP) plots show the 16 clusters of PBMCs identified by FindClusters and the final annotation of single-cell clusters to the immune cell types: natural killer (NK) cells, monocytes, platelets, B cells, T cells, and red blood cells; 13662 randomly selected cells are shown in each final-annotated plot for comparability. **G**, Stacked bar plots show percentages of the annotated immune cell types as mean per group (cohort 3). **H**, The dot plot shows scaled average expression (color) of orthologous of Figure 1H (here: cohort 3). Scaled average expression refers to *Z* score normalized gene expression values. This standardization centers the values on 0 and scales the variance to 1. Dot size indicates the percentage of cells expressing each gene scaled by the maximal percentage per gene. **I**, Bulk RNA sequencing was performed of RNA isolated from PBMCs of a subset of mice shown in **A** (cohort 4; control: n=5; HFpEF: n=5; and HFpEF+NO_2-OA: n=6). Heat map shows scaled average expression (color) of genes shown in **H**. Scaled average expression refers to *Z* score normalized gene expression values. This standardization centers the values on 0 and scales the variance to 1. **J**, OrthoIntegrate was used to assign orthologues and integrate single-cell data from human (cohort 1) and mouse PBMCs (cohort 3; both cohorts: control and HFpEF, lean [l]+obese [o]). Differentially expressed genes (DEGs; up+down) between HFpEF (l+o) and Control (l+o) were then identified for each cell type and species using FindMarkers (Wilcoxon rank-sum test, Bonferroni-corrected $P<0.05$). Sankey plot shows the percentage of species-specific and shared orthologue DEGs per cell type. **K**, Density plots show the density of cells expressing selected genes from Figure 1F (Venn diagram, ↑ HFpEF) and their mouse orthologue (cohort 1+cohort 3). Blue indicates high expression density, and white indicates low expression density. Dot plots (**L**: cohort 1, human; **M**: cohort 3, mouse) display selected genes of Figure 1F (Venn diagram, ↑ HFpEF), percentage of cells expressing each gene scaled by the maximal percentage per gene (dot size), and scaled average expression among each gene (dot color). Scaled average expression refers to *Z* score normalized gene expression values. This standardization centers the values on 0 and scales the variance to 1. Legend applies to both dot plots. **N**, For validation of scRNA-seq data from human PBMCs, bulk RNA sequencing was performed of RNA isolated from whole blood of controls (n=8), patients with heart failure with reduced ejection fraction (HFrEF; ischemic, n=5; nonischemic: n=11), and patients with HFpEF (n=18; cohort 2). Heat map shows scaled average expression (color) of genes shown in **L**. Scaled average expression refers to *Z* score normalized gene expression values. This standardization centers the values on 0 and scales the variance to 1. **O**, For validation of scRNA-seq data from mouse PBMCs, bulk RNA sequencing was performed of RNA isolated from PBMCs of a subset of mice shown in **A** (cohort 4; control: n=5; HFpEF: n=5; and HFpEF+NO_2-OA: n=6). Heat map shows scaled average expression (color) of genes shown in **M**. Scaled average expression refers to *Z* score normalized gene expression values. This standardization centers the values on 0 and scales the variance to 1. **A**, **F**, **I**, and **L** through **O** were drawn in part using images from Servier Medical Art. Servier Medical Art by Servier is licensed under a Creative Commons Attribution 3.0 Unported License (https://creativecommons.org/licenses/by/3.0/).

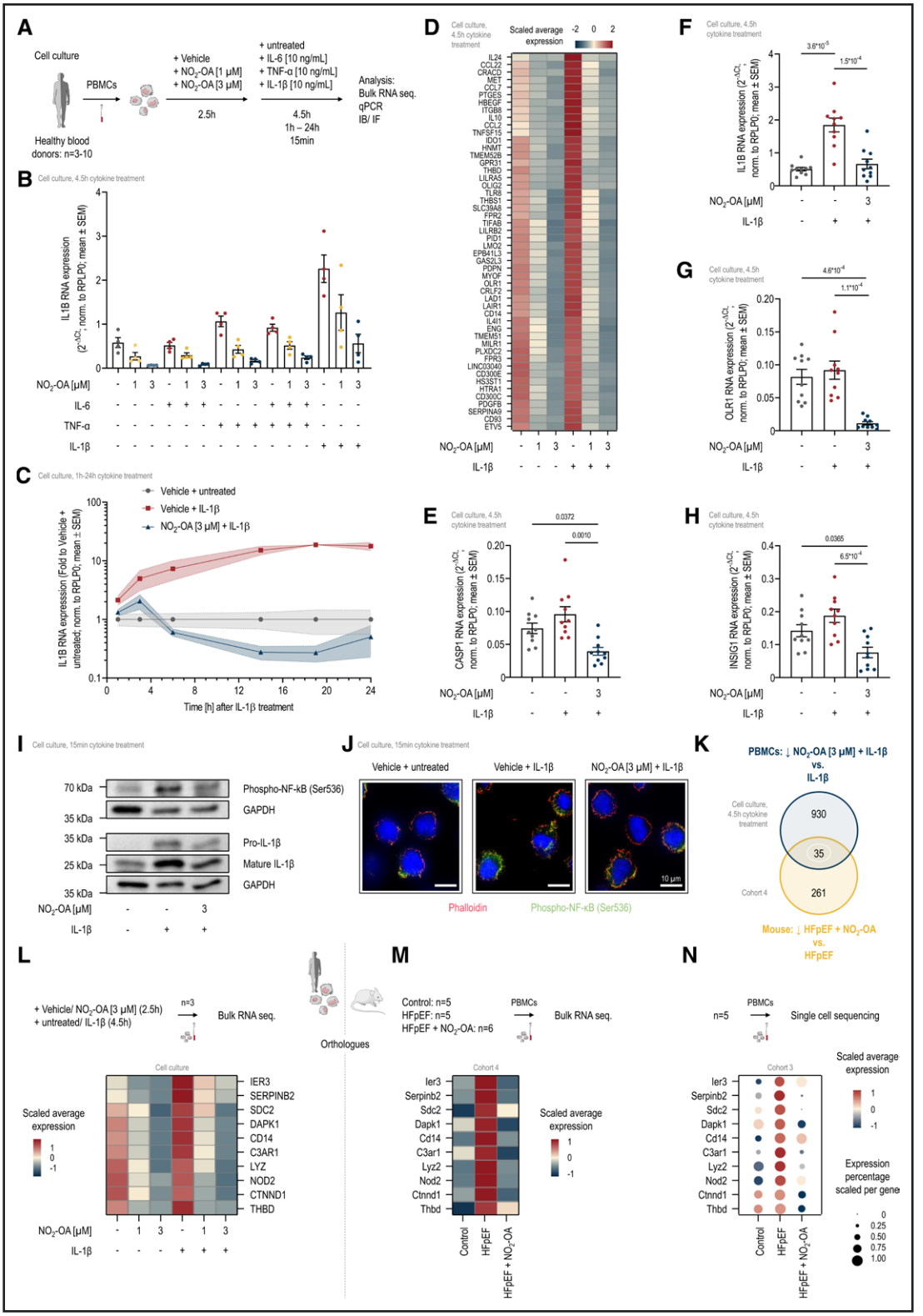

Figure 3. Nitro-oleic acid (NO_2-OA) treatment reduces the inflammatory response of human immune cells.
A, Schematic illustration of experiments performed on the functional mechanism of NO_2-OA: peripheral blood mononuclear cells (PBMCs) were isolated from healthy blood donors and then treated with vehicle or NO_2-OA (1 or 3 µmol/L) for 2.5 hours. Furthermore, PBMCs were either left untreated or treated with IL (interleukin)-6 (10 ng/mL), TNF-α (tumor necrosis factor alpha; 10 ng/mL), IL-1β (10 ng/mL), or a combination of IL-6 (10 ng/mL) and TNF-α (10 ng/mL). Quantitative polymerase chain reaction (qPCR)/bulk RNA sequencing (n=3; 4.5-hour cytokine treatment), qPCR (n=3–4 [19 hours, n=3]; 1–24-hour cytokine treatment), qPCR (n=10; 4.5-hour cytokine treatment), and WB/IF (15-minute cytokine treatment) were performed. For immune fluorescence experiments, THP1 cells were used instead of primary human (*Continued*)

with HFrEF, further delineating the immune landscape of HFpEF.

Mitochondrial dysfunction in HFpEF appears to be another key differentiator from HFrEF and is tightly entwined with inflammation. Mounting evidence indicates that HFpEF hearts have a fundamental energetic impairment and metabolic inflexibility. In a recent study, HFpEF myocardial tissue showed greater reliance on fatty acid oxidation, with limited ability to switch to alternative fuels, contrasted with the metabolic profile of HFrEF. Concomitantly, HFpEF hearts failed to activate protective mitophagy despite significant mitochondrial oxidative stress, whereas hearts from obese-but-nonfailing models did upregulate mitophagy.[28] This maladaptive response in HFpEF leads to the accumulation of dysfunctional mitochondria and excess reactive oxygen species, which can further amplify inflammatory signaling. Our transcriptomic analysis of HFpEF PBMCs revealed signatures consistent with this paradigm, for example, altered expression of genes governing mitochondrial respiration and redox homeostasis, suggesting that circulating immune cells mirror the mitochondrial stress seen in the myocardium. Such frustrated mitochondria in immune cells might drive proinflammatory activation, linking metabolic dysfunction to systemic inflammation in HFpEF.[29] Importantly, treatment with NO_2-OA favorably modulated both immune and mitochondrial pathways in our HFpEF model, highlighting a potential therapeutic avenue. Herein, NO_2-OA induced an improvement of diastolic function and an alleviation of heart failure symptoms.[12] However, whether the modulation of PBMC phenotype is causally related to these effects remains elusive. Although these effects were observed exclusively in the mouse model, we think that our data have translational relevance to humans, given that NO_2-OA has been shown to not only exert a positive safety and tolerability profile in healthy and obese subjects but also reduce plasma cytokine levels in individuals with obesity.[30] Based on the positive results of phase I studies, a phase II trial is currently being conducted in obese asthmatics to test the anti-inflammatory, tissue metabolic, microbiome, and pulmonary function actions of NO_2-OA in this patient cohort (Unique identifier: NCT03762395). The clinical observations together with the preclinical evidence of anti-inflammatory actions support the translational potential of this molecule. NO_2-OA is known to exert broad anti-inflammatory effects by covalently modifying key signaling proteins.[31,32] For example, recent work demonstrated that NO_2-OA can nitroalkylate the phosphatase calcineurin in T cells, thereby inhibiting NFAT-mediated proinflammatory gene expression and T-cell activation.[33] In our study, HFpEF mice treated with NO_2-OA showed a blunting of systemic inflammatory responses: proinflammatory cytokine expression and leukocyte activation markers were reduced compared with untreated HFpEF, indicating restoration of a more quiescent immune state. In parallel, NO_2-OA markedly improved mitochondrial-related gene expression and metabolism. This aligns with findings that

Figure 3 Continued. PBMCs. **B**, RNA expression of *IL1B* in PBMCs after pretreatment with NO_2-OA (1 or 3 µmol/L) for 2.5 hours and subsequent cytokine treatment (each cytokine: 10 ng/mL) for 4.5 hours measured by qPCR (n=4, cell culture). **C**, RNA expression of *IL1B* in PBMCs after pretreatment with NO_2-OA (3 µmol/L) for 2.5 hours and subsequent IL-1β treatment (10 ng/mL) for 1 (n=4), 3 (n=4), 6 (n=4), 14 (n=4), 19 (n=3), or 24 hours (n=4) measured by qPCR (n=3–4, cell culture). **D** through **H**, PBMCs were pretreated with NO_2-OA (1 or 3 µmol/L) for 2.5 hours and then treated with IL-1β (10 ng/mL) for 4.5 hours. Bulk RNA sequencing was performed (n=3, cell culture). Using edgeR, differentially expressed genes (exact negative binomial test; $P<0.05$) were identified. **D**, Heat map shows selection of genes significantly upregulated after IL-1β treatment and downregulated with NO_2-OA (3 µmol/L) treatment prior to IL-1β treatment. Scaled average expression refers to *Z* score normalized gene expression values. This standardization centers the values on 0 and scales the variance to 1. Bar graphs show RNA expression of (**E**) CASP1 (caspase-1), (**F**) IL1B, (**G**) OLR1 (oxidized low-density lipoprotein receptor 1), and (**H**) INSIG1 (insulin induced gene 1; qPCR; n=10, cell culture; all: RM 1-way ANOVA followed by the Tukey multiple comparisons test, with a single pooled variance). **I**, PBMCs were pretreated with NO_2-OA (3 µmol/L) for 2.5 hours and then treated with IL-1β (10 ng/mL) for 15 minutes. Subsequent immunoblotting for phospho-NF-κB (Ser536), pro-IL-1β, mature IL-1β, and GAPDH (loading control) was performed. **J**, THP1 cells were pretreated with NO_2-OA (3 µmol/L) for 2.5 hours and then treated with IL-1β (10 ng/mL) for 15 minutes. Cells were subsequently fixed and processed for immunofluorescence staining using phospho-NF-κB (Ser536) and acti-stain 555 phalloidin antibodies. Nuclei were counterstained with Hoechst dye. Images were acquired using a 63× oil immersion objective. Scale bar, 10 µm. **K**, Cell culture: PBMCs were pretreated with NO_2-OA (3 µmol/L) for 2.5 hours and then treated with IL-1β (10 ng/mL) for 4.5 hours. Bulk RNA sequencing was performed (n=3, cell culture). Using edgeR, differentially expressed genes (exact negative binomial test; $P<0.05$) were identified, which were downregulated when pretreated with NO_2-OA (3 µmol/L) before IL-1β treatment compared with IL-1β treatment following prior vehicle treatment. Cohort 4: for validation of single-cell RNA sequencing (scRNA-seq) data from mouse PBMCs, bulk RNA sequencing was performed of RNA isolated from PBMCs of a subset of mice shown in Figure 2A (cohort 4; control: n=5; heart failure with preserved ejection fraction [HFpEF]: n=5; and HFpEF+NO_2-OA: n=6). Using edgeR, differentially expressed genes (exact negative binomial test; $P<0.05$) were identified, which were downregulated in HFpEF+NO_2-OA mice compared with HFpEF mice. A Venn diagram shows the number of genes significantly downregulated by NO_2-OA in the cell culture experiment and the HFpEF animal model (cohort 4), as well as orthologue overlaps. **L** and **M**, Heat maps show scaled average expression (color) of selection of genes jointly downregulated by NO_2-OA (**K** and **L**: cell culture, human PBMCs; **M**: cohort 4, mouse, bulk sequencing). Scaled average expression refers to *Z* score normalized gene expression values. This standardization centers the values on 0 and scales the variance to 1. **N**, The dot plot displays genes shown in **M**, now in the scRNA-seq data set of cohort 3, percentage of cells expressing each gene scaled by the maximal percentage per gene (dot size) and scaled average expression among each gene (dot color). Scaled average expression refers to *Z* score normalized gene expression values. This standardization centers the values on 0 and scales the variance to 1. **A** and **L** through **N** were drawn in part using images from Servier Medical Art. Servier Medical Art by Servier is licensed under a Creative Commons Attribution 3.0 Unported License (https://creativecommons.org/licenses/by/3.0/). Bar graphs are presented as mean±SEM.

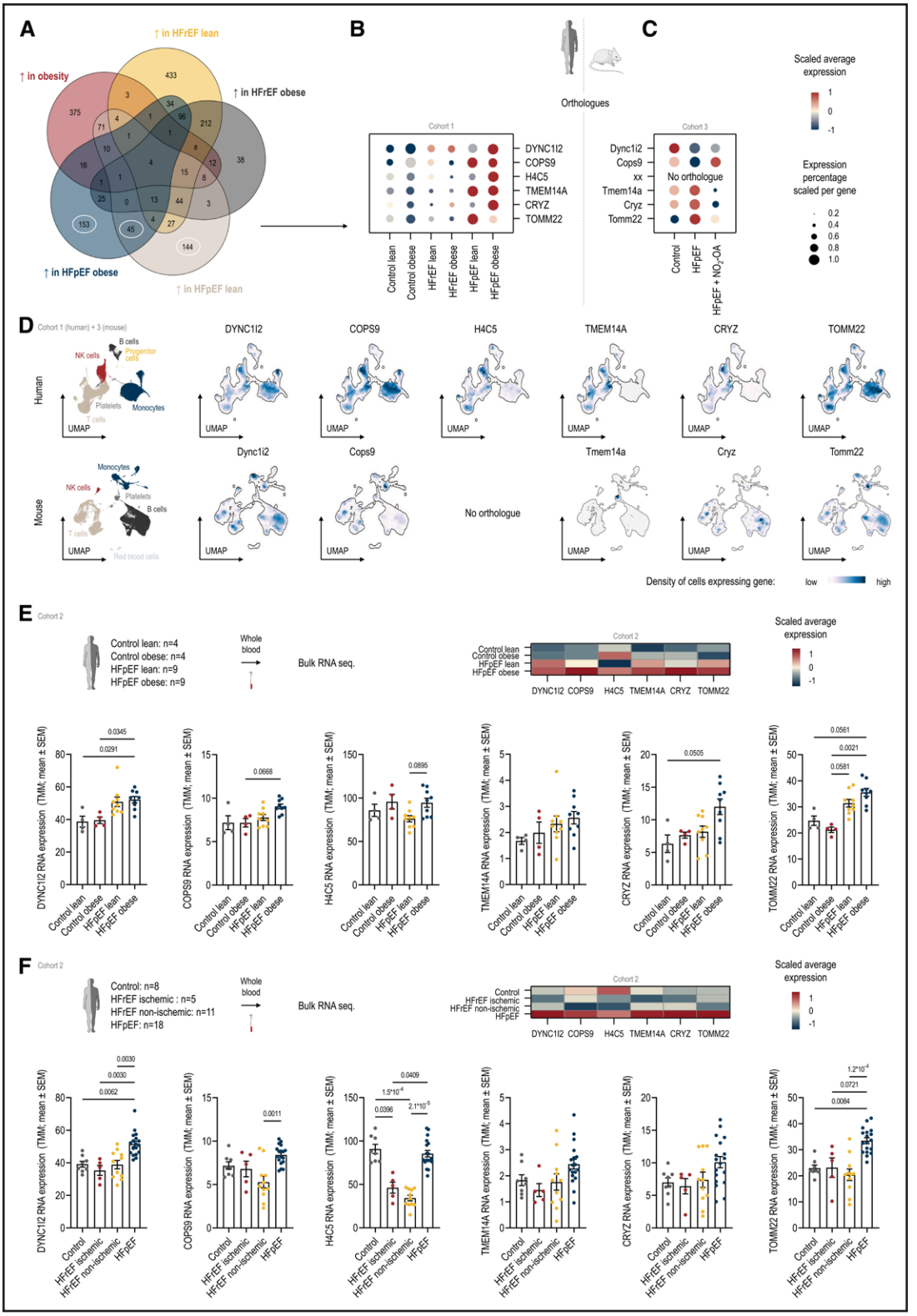

Figure 4. Validation of identified differentially expressed genes (DEGs) in a human heart failure with preserved ejection fraction (HFpEF) cohort.

A, Using FindMarkers (logfc.threshold=0.5, min.pct=0.05, and only.pos=TRUE), differentially expressed genes (DEGs) between control obese and control lean, heart failure with reduced ejection fraction (HFrEF) lean and control lean, HFrEF obese and control lean, HFpEF lean and control lean, and HFpEF obese and control lean were identified (cohort 1). A Venn diagram shows the number of significantly upregulated genes (Wilcoxon rank-sum test, Bonferroni-corrected $P<0.05$) in each disease separated by body mass index (BMI: lean: <30 kg/m^2 and obese: >30 kg/m^2) and overlaps. **B** and **C**, Dot plots (**B**: cohort 1, human, single-cell RNA sequencing [scRNA-seq]; **C**: cohort 3, mouse, (*Continued*)

Figure 4 Continued. scRNA-seq) display selected genes of **A** (Venn diagram, only ↑ HFpEF), percentage of cells expressing each gene scaled by the maximal percentage per gene (dot size), and scaled average expression among each gene (dot color). Scaled average expression refers to *Z* score normalized gene expression values. This standardization centers the values on 0 and scales the variance to 1. Legend applies to both dot plots. No orthologues were found for H4C5. **D**, Density plots show the density of cells expressing selected genes shown in **B** (Venn diagram, only ↑ HFpEF) and their mouse orthologue (cohort 1+cohort 3). Blue indicates high expression density, and white indicates low expression density. **E**, For validation of scRNA-seq data from human peripheral blood mononuclear cells (PBMCs), bulk RNA sequencing was performed of RNA isolated from whole blood of lean (n=4) and obese (n=4) controls, and lean patients (n=9) and patients with obesity (n=9) with HFpEF (cohort 2). Heat map shows scaled average expression (color) of genes shown in **B**. Scaled average expression refers to *Z* score normalized gene expression values. This standardization centers the values on 0 and scales the variance to 1. Bar graphs show RNA expression of genes shown in **B** (all: trimmed mean of M values [TMM]; all: Kruskal-Wallis test followed by the Dunn multiple comparisons test). **F**, For validation of scRNA-seq data from human PBMCs, bulk RNA sequencing was performed of RNA isolated from whole blood of controls (n=8) and patients with HFrEF (ischemic: n=5 and nonischemic: n=11) and HFpEF (n=18; cohort 2). Heat map shows scaled average expression (color) of genes shown in **B**. Scaled average expression refers to *Z* score normalized gene expression values. This standardization centers the values on 0 and scales the variance to 1. Bar graphs show RNA expression of genes shown in **B** (all: TMM; all: Kruskal-Wallis test followed by the Dunn multiple comparisons test). **B**, **C**, **E**, and **F** were drawn in part using images from Servier Medical Art. Servier Medical Art by Servier is licensed under a Creative Commons Attribution 3.0 Unported License (https://creativecommons.org/licenses/by/3.0/). Bar graphs are presented as mean±SEM. UMAP indicates uniform manifold approximation and projection.

a 4-week NO_2-OA treatment in a diet-induced HFpEF mouse model enhanced cardiac mitochondrial biogenesis and oxidative phosphorylation capacity via activation of the AMPK pathway.[11] We observed analogous improvements, including upregulation of mitochondrial proteins and attenuation of oxidative stress signatures in immune cells. Thus, NO_2-OA appears to break the detrimental cycle of metabolic inflammation in HFpEF, simultaneously dampening inflammation and bolstering mitochondrial function.

From a translational perspective, our results provide important insights and future directions. First, by demonstrating that peripheral blood immune cells reflect the inflammatory and metabolic derangements of HFpEF, we support the use of blood-based biomarkers or transcriptomic profiles for individual patient phenotyping. This could enable identification of an inflamed HFpEF endotype that might respond to targeted anti-inflammatory or metabolic therapies. We identified previously undescribed genes that are specifically regulated in HFpEF, including many genes related to the mitochondrion or energy production, such as *CRYZ*, *TMEM14A*, or *TOMM22*, which have not been previously described in the context of HFpEF but are associated with stressed myocardium.[34] Second, our work highlights immunometabolic pathways, such as inflammatory cytokine signaling, oxidative stress, and mitochondrial quality control, as promising therapeutic targets in HFpEF. The salutary effects of NO_2-OA in our preclinical model suggest that therapies aiming to reduce inflammation and improve metabolic flexibility can ameliorate HFpEF features. This concept is bolstered by clinical trial findings that agents with metabolic and anti-inflammatory benefits (eg, SGLT2 inhibitors) improve outcomes in HFpEF.[35] Finally, we acknowledge that inflammation in HFpEF is complex and multiorgan. Our focus on circulating cells provides a holistic view, but certain localized processes (for instance, in the myocardium, spleen, or adipose tissue) were beyond the scope of this study. Future investigations integrating myocardial and peripheral immune profiling will further elucidate the cross talk between compartments.

This study has several limitations. The cohort sizes were small, especially in the scRNA-seq arm. In addition, the use of observational data reduces direct causal inference. The observations should, therefore, be verified in larger, unselected cohorts. Although the HFpEF mouse model recapitulates important phenotypic features, it also shows differences, and its generalizability to the heterogeneity of human HFpEF is limited. Furthermore, our analysis was limited to circulating immune cells, while tissue- and organ-specific immune responses (eg, cardiac macrophages, splenic reservoirs, and adipose inflammation) were not considered. Future studies integrating spatial transcriptomics and plasma cytokine profiling may shed more light on the interplay between systemic and myocardial inflammation in HFpEF.

In conclusion, our study describes systemic immune activation and mitochondrial dysfunction as features more common in the group of patients with HFpEF than in those with HFrEF and demonstrates that an immunometabolic modulator such as NO_2-OA showed a favorable result in a mouse model of HFpEF due to high-fat diet and L-NAME and may be potentially explored as a therapeutic strategy for patients with HFpEF.

ARTICLE INFORMATION

Received February 4, 2025; revision received June 17, 2025; accepted June 20, 2025.

Affiliations

Klinik und Poliklinik für Kardiologie, Universitätsklinikum Leipzig, Germany (J.M.K., S.E., K.E.K., I.M.-K., S.C.S., C.M., S.F.H., S.G., R.W., U.L., J.-N.B.). Central German Heart Alliance (J.M.K., S.E., K.E.K., I.M.-K., S.C.S., C.M., S.F.H., S.G., R.W., U.L., J.-N.B.). Clinic for General and Interventional Cardiology/Angiology (M.M., A.K.) and Agnes Wittenborg Institute for Translational Cardiovascular Research, Herz- und Diabeteszentrum NRW, Ruhr-Universität Bochum, Germany (M.M., A.K.). Department of Cardiology, Heart Center at University of Leipzig, Germany (S.R., P.L.). Department of Cardiology, Universitätsmedizin Johannes Gutenberg-University, Mainz, Germany (S.R., P.L.). Department of Cardiology and Pneumology, University Medical Center of Göttingen, Germany (S.v.H.). German Center for Cardiovascular Research (DZHK) (S.v.H.). Medical Department III-Endocrinology, Nephrology,

Rheumatology, University of Leipzig Medical Center, Germany (A.T., M.B.). Helmholtz Institute for Metabolic, Obesity and Vascular Research of the Helmholtz Zentrum München, University of Leipzig and University Hospital Leipzig, Germany (M.B.).

Acknowledgments

The authors thank Tino Röxe and Anne Marie Müller for excellent technical support. Nitro-oleic acid was kindly provided by Bruce A. Freeman, University of Pittsburgh, PA.

Sources of Funding

This work was funded by the German Research Foundation (Deutsche Forschungsgemeinschaft) under project 512725688 to J.-N. Boeckel, project MU 4726/2-1 to M. Müller, and project KL 2516/5-1 to A. Klinke.

Disclosures

None.

Supplemental Material

Supplemental Figures
Excel S1
Major Resources Table
Unedited Blots

REFERENCES

1. Alcaide P, Kallikourdis M, Emig R, Prabhu SD. Myocardial inflammation in heart failure with reduced and preserved ejection fraction. *Circ Res*. 2024;134:1752–1766. doi: 10.1161/CIRCRESAHA.124.323659
2. Lanzer JD, Valdeolivas A, Pepin M, Hund H, Backs J, Frey N, Friederich HC, Schultz JH, Saez-Rodriguez J, Levinson RT. A network medicine approach to study comorbidities in heart failure with preserved ejection fraction. *BMC Med*. 2023;21:267. doi: 10.1186/s12916-023-02922-7
3. Adamo L, Rocha-Resende C, Prabhu SD, Mann DL. Reappraising the role of inflammation in heart failure. *Nat Rev Cardiol*. 2020;17:269–285. doi: 10.1038/s41569-019-0315-x
4. Franssen C, Chen S, Unger A, Korkmaz HI, De Keulenaer GW, Tschöpe C, Leite-Moreira AF, Musters R, Niessen HWM, Linke WA, et al. Myocardial microvascular inflammatory endothelial activation in heart failure with preserved ejection fraction. *JACC Heart Fail*. 2016;4:312–324. doi: 10.1016/j.jchf.2015.10.007
5. Hahn VS, Yanek LR, Vaishnav J, Ying W, Vaidya D, Lee YZJ, Riley SJ, Subramanya V, Brown EE, Hopkins CD, et al. Endomyocardial biopsy characterization of heart failure with preserved ejection fraction and prevalence of cardiac amyloidosis. *JACC Heart Fail*. 2020;8:712–724. doi: 10.1016/j.jchf.2020.04.007
6. Kolijn D, Pabel S, Tian Y, Lódi M, Herwig M, Carrizzo A, Zhazykbayeva S, Kovács A, Fülöp GA, Falcão-Pires I, et al. Empagliflozin improves endothelial and cardiomyocyte function in human heart failure with preserved ejection fraction via reduced pro-inflammatory-oxidative pathways and protein kinase Gα oxidation. *Cardiovasc Res*. 2021;117:495–507. doi: 10.1093/cvr/cvaa123
7. Ye B, Bradshaw AD, Abrahante JE, Dragon JA, Häußler TN, Bell SP, Hirashima F, LeWinter M, Zile MR, Meyer M. Left Ventricular gene expression in heart failure with preserved ejection fraction—profibrotic and proinflammatory pathways and genes. *Circ Hear Fail*. 2023;16. doi: 10.1161/circheartfailure.123.010395
8. Ye B, Bradshaw AD, Abrahante JE, Dragon JA, Häußler TN, Bell SP, Hirashima F, LeWinter M, Zile MR, Meyer M. Left ventricular gene expression in heart failure with preserved ejection fraction-profibrotic and proinflammatory pathways and genes. *Circ Heart Fail*. 2023;16:e010395. doi: 10.1161/CIRCHEARTFAILURE.123.010395
9. Eidizadeh A, Schnelle M, Leha A, Edelmann F, Nolte K, Werhahn SM, Binder L, Wachter R. Biomarker profiles in heart failure with preserved vs. reduced ejection fraction: results from the DIAST-CHF study. *ESC Heart Fail*. 2023;10:200–210. doi: 10.1002/ehf2.14167
10. Schiattarella GG, Altamirano F, Tong D, French KM, Villalobos E, Kim SY, Luo X, Jiang N, May HI, Wang ZV, et al. Nitrosative stress drives heart failure with preserved ejection fraction. *Nature*. 2019;568:351–356. doi: 10.1038/s41586-019-1100-z
11. Müller M, Schubert T, Welke C, Schulz TJ, Patschkowski T, Maske T, Lengenfelder LA, Landwehrjohann L, Donhauser E, Vogt ET, et al. Enhanced cardiac mitochondrial biogenesis by nitro-oleic acid remedies diastolic dysfunction in a mouse model of heart failure with preserved ejection fraction. *bioRxiv*. 2024;2024-02.
12. Müller M, Schubert T, Welke C, Maske T, Patschkowski T, Donhauser E, Heinen-Weiler J, Hormann F-L, Heiles S, Schulz TJ, et al. Nitro-oleic acid enhances mitochondrial metabolism and ameliorates heart failure with preserved ejection fraction in mice. *Nat Commun*. 2025;16:3933. doi: 10.1038/s41467-025-59192-5
13. Aran D, Looney AP, Liu L, Wu E, Fong V, Hsu A, Chak S, Naikawadi RP, Wolters PJ, Abate AR, et al. Reference-based analysis of lung single-cell sequencing reveals a transitional profibrotic macrophage. *Nat Immunol*. 2019;20:163–172. doi: 10.1038/s41590-018-0276-y
14. Stürzebecher PE, Kralisch S, Schubert MR, Filipova V, Hoffmann A, Oliveira F, Sheikh BN, Blüher M, Kogel A, Scholz M, et al. Leptin treatment has vasculo-protective effects in lipodystrophic mice. *Proc Natl Acad Sci USA*. 2022;119:e2110374119. doi: 10.1073/pnas.2110374119
15. Kokot KE, Kneuer JM, John D, Rebs S, Möbius-Winkler MN, Erbe S, Müller M, Andritschke M, Gaul S, Sheikh BN, et al. Reduction of A-to-I RNA editing in the failing human heart regulates formation of circular RNAs. *Basic Res Cardiol*. 2022;117:32. doi: 10.1007/s00395-022-00940-9
16. Tsang M, Gantchev J, Ghazawi FM, Litvinov IV. Protocol for adhesion and immunostaining of lymphocytes and other non-adherent cells in culture. *Biotechniques*. 2017;63:230–233. doi: 10.2144/000114610
17. Kneuer JM, Grajek IA, Winkler M, Erbe S, Meinecke T, Weiss R, Garfias-Veitl T, Sheikh BN, König AC, Möbius-Winkler MN, et al. Novel long noncoding RNA HEAT4 affects monocyte subtypes, reducing inflammation and promoting vascular healing. *Circulation*. 2024;150:1101–1120. doi: 10.1161/circulationaha.124.069315
18. Smart CD, Madhur MS. The immunology of heart failure with preserved ejection fraction. *Clin Sci (Lond)*. 2023;137:1225–1247. doi: 10.1042/CS20230226
19. Hassoun R, Hamdani N. Inflammation in HFpEF: crucial or ancillary? *Circ Hear Fail*. 2023;16:e010887. doi: 10.1161/CIRCHEARTFAILURE.123.010887
20. Schiattarella GG, Rodolico D, Hill JA. Metabolic inflammation in heart failure with preserved ejection fraction. *Cardiovasc Res*. 2021;117:423–434. doi: 10.1093/cvr/cvaa217
21. Schiattarella GG, Alcaide P, Condorelli G, Gillette TG, Heymans S, Jones EAV, Kallikourdis M, Lichtman A, Marelli-Berg F, Shah SJ, et al. Immunometabolic mechanisms of heart failure with preserved ejection fraction. *Nat Cardiovasc Res*. 2022;1:211–222. doi: 10.1038/s44161-022-00032-w
22. DuBrock HM, AbouEzzeddine OF, Redfield MM. High-sensitivity C-reactive protein in heart failure with preserved ejection fraction. *PLoS One*. 2018;13:e0201836. doi: 10.1371/journal.pone.0201836
23. Li N, Bian H, Zhang J, Li X, Ji X, Zhang Y. The Th17/Treg imbalance exists in patients with heart failure with normal ejection fraction and heart failure with reduced ejection fraction. *Clin Chim Acta*. 2010;411:1963–1968. doi: 10.1016/j.cca.2010.08.013
24. Strocchi S, Liu L, Wang R, Häseli SP, Capone F, Bode D, Nambiar N, Eroglu T, Santiago Padilla L, Farrelly C, et al. Systems biology approach uncovers candidates for liver-heart interorgan crosstalk in HFpEF. *Circ Res*. 2024;135:873–876. doi: 10.1161/CIRCRESAHA.124.324829
25. Mazzotta C, Basu S, Gower AC, Karki S, Farb MG, Sroczynski E, Zizza E, Sarhan A, Pande AN, Walsh K, et al. Perivascular adipose tissue inflammation in ischemic heart disease. *Arterioscler Thromb Vasc Biol*. 2021;41:1239–1250. doi: 10.1161/ATVBAHA.120.315865
26. Ouwens DM, Sell H, Greulich S, Eckel J. The role of epicardial and perivascular adipose tissue in the pathophysiology of cardiovascular disease. *J Cell Mol Med*. 2010;14:2223–2234. doi: 10.1111/j.1582-4934.2010.01141.x
27. Andrzejczyk K, Abou Kamar S, van Ommen A-M, Canto ED, Petersen TB, Valstar G, Akkerhuis KM, Cramer MJ, Umans V, Rutten FH, et al. Identifying plasma proteomic signatures from health to heart failure, across the ejection fraction spectrum. *Sci Rep*. 2024;14:14871. doi: 10.1038/s41598-024-65667-0
28. Yoshii A, McMillen TS, Wang Y, Zhou B, Chen H, Banerjee D, Herrero M, Wang P, Muraoka N, Wang W, et al. Blunted cardiac mitophagy in response to metabolic stress contributes to HFpEF. *Circ Res*. 2024;135:1004–1017. doi: 10.1161/CIRCRESAHA.123.324103
29. Filipp M, Ge Z-D, DeBerge M, Lantz C, Glinton K, Gao P, Smolgovsky S, Dai J, Zhao Y-Y, Yvan-Charvet L, et al. Myeloid fatty acid metabolism activates neighboring hematopoietic stem cells to promote heart failure with preserved ejection fraction. *Circulation*. 2025;151:1451–1466. doi: 10.1161/CIRCULATIONAHA.124.070248
30. Garner RM, Mould DR, Chieffo C, Jorkasky DK. Pharmacokinetic and pharmacodynamic effects of oral CXA-10, a nitro fatty acid, after single and

multiple ascending doses in healthy and obese subjects. *Clin Transl Sci.* 2019;12:667–676. doi: 10.1111/cts.12672
31. Rudolph TK, Rudolph V, Edreira MM, Cole MP, Bonacci G, Schopfer FJ, Woodcock SR, Franek A, Pekarova M, Khoo NKH, et al. Nitro–fatty acids reduce atherosclerosis in apolipoprotein E–deficient mice. *Arterioscler Thromb Vasc Biol.* 2010;30:938–945. doi: 10.1161/ATVBAHA.109.201582
32. Rudolph V, Rudolph TK, Schopfer FJ, Bonacci G, Woodcock SR, Cole MP, Baker PRS, Ramani R, Freeman BA. Endogenous generation and protective effects of nitro-fatty acids in a murine model of focal cardiac ischaemia and reperfusion. *Cardiovasc Res.* 2010;85:155–166. doi: 10.1093/cvr/cvp275
33. Bago A, Cayuela ML, Gil A, Calvo E, Vázquez J, Queiro A, Schopfer FJ, Radi R, Serrador JM, Íñiguez MA. Nitro-oleic acid regulates T cell activation through post-translational modification of calcineurin. *Proc Natl Acad Sci.* 2023;120:e2208924120. doi: 10.1073/pnas.2208924120
34. Bose HS, Whittal RM, Marshall B, Rajapaksha M, Wang NP, Bose M, Perry EW, Zhao Z-Q, Miller WL. A novel mitochondrial complex of aldosterone synthase, steroidogenic acute regulatory protein, and Tom22 synthesizes aldosterone in the rat heart. *J Pharmacol Exp Ther.* 2021;377:108–120. doi: 10.1124/jpet.120.000365
35. Heidenreich PA, Bozkurt B, Aguilar D, Allen LA, Byun J-J, Colvin MM, Deswal A, Drazner MH, Dunlay SM, Evers LR, et al; Writing Committee Members. 2022 ACC/AHA/HFSA guideline for the management of heart failure: executive summary. *J Card Fail.* 2022;28:810–830. doi: 10.1016/j.cardfail.2022.02.009